

# Bragg spectroscopy of a strongly interacting $^{85}\text{Rb}$ Bose-Einstein condensate

S. B. Papp,<sup>1</sup> J. M. Pino,<sup>1</sup> R. J. Wild,<sup>1</sup> S. Ronen,<sup>1</sup> C. E. Wieman,<sup>2,1</sup> D. S. Jin,<sup>1</sup> and E. A. Cornell<sup>1,\*</sup>

<sup>1</sup>*JILA, Quantum Physics Division, National Institute of Standards and Technology and Department of Physics, University of Colorado, Boulder, Colorado 80309-0440, USA*

<sup>2</sup>*University of British Columbia, Vancouver, BC V6T 1Z1, Canada*

(Dated: October 24, 2018)

We report on measurements of the excitation spectrum of a strongly interacting Bose-Einstein condensate (BEC). A magnetic-field Feshbach resonance is used to tune atom-atom interactions in the condensate and to reach a regime where quantum depletion and beyond mean-field corrections to the condensate chemical potential are significant. We use two-photon Bragg spectroscopy to probe the condensate excitation spectrum; our results demonstrate the onset of beyond mean-field effects in a gaseous BEC.

The concept of an interacting but dilute Bose gas was originally developed fifty years ago as a theoretically tractable surrogate for superfluid liquid helium. For some years after the eventual experimental realization of dilute-gas BEC, experiments were performed mainly in the extreme dilute limit, in which atom-atom correlations were of negligible significance. Such correlations again assumed a central role, however, in the 2002 experiments on a Mott state for bosons in an optical lattice [1] and on atom-molecule coherence near a Feshbach resonance [2]. Atom-atom correlations are also central to the current hot-topic field of resonant fermionic condensates [3, 4].

In this paper we describe an experimental study of elementary excitations in a system which harkens back to a previous century, in that, like liquid helium, it is a strongly interacting, bulk, bosonic superfluid. Unlike liquid helium, our gas of Bose-condensed  $^{85}\text{Rb}$  has the modern virtue of Feshbach-tunable interactions well-described by a scattering length  $a$  that is much larger than the reach of the actual interatomic potential. Our primary tool for characterizing the sample is Bragg spectroscopy [5, 6].

The convenience of a Feshbach-tunable scattering length in a bosonic system comes at a cost: at high values of  $na^3$  the gas decays relatively quickly. For this reason, we are not able to use, for example, shifts in breathing-mode frequencies [7] that have been so fruitful in the resonant fermion systems [8, 9]. These measurements require that the gas survive at least as long as it takes to traverse the sample at the speed of sound. Bragg scattering, on the other hand, is essentially a local measurement. The magnetic field can be ramped to tune the sample to a large scattering length, and the Bragg pulse can be applied on a time scale faster than that required for global equilibrium but still consistent with local many-body quasi-equilibrium.

What should we expect for the energy,  $\hbar\omega(k)$ , of an excitation with momentum  $\hbar k$  above a Bose-Einstein condensate of homogeneous density  $n$ ? In the absence of any interactions, the energy of the excitation is simply  $\hbar^2 k^2 / (2m)$ , where  $m$  is the mass of an atom. In the sim-

plest description of interactions, atoms in the condensate feel a chemical potential,  $\mu = 4\pi\hbar^2 na/m$  [10]. On the other hand, a high momentum excitation has equal direct and exchange interactions, of magnitude  $\mu$  each, with the low momentum atoms. Thus, the energy required to promote an atom out of the condensate, less the bare kinetic energy, is

$$\hbar\omega(k) - \frac{\hbar^2 k^2}{2m} = 2\mu - \mu = \frac{4\pi\hbar^2 na}{m}. \quad (1)$$

The simple model leading to this energy shift, linear in  $n$  and  $a$  (see Fig. 1), relies implicitly on the smallness of three dimensionless parameters, which are the following:

1.  $\sqrt{8\pi na^3} \ll 1$ , so that interactions are amenable to a mean-field treatment.
2.  $ka \ll 1$ , so that the two-body scattering amplitude is momentum independent.
3.  $1/(k\xi) \ll 1$ , where  $\xi = \hbar/(2m\mu)^{1/2}$  is the healing length. This limit corresponds to the excitation being cleanly in the free-particle regime. For larger  $1/(k\xi)$ , the excitation becomes more of a collective object until, in the opposite limit  $1/(k\xi) \gg 1$ , the excitation is a phonon. The crossover regime was studied experimentally [11, 12] with the results confirming the original theory by Bogoliubov [13].

The primary goal of the work reported in this paper is to push into a regime where interactions in a cold Bose gas *can't* be treated as a mean field. For our data the next order, Lee Huang Yang (LHY) correction  $\alpha \equiv \frac{32}{3\pi\sqrt{8}}\sqrt{8\pi na^3}$  [14, 15] is as large as 0.5. As we increase  $a$ , the parameters 2 and 3 will also increase. For the data presented in this paper  $1/(k\xi) < 0.5$  and  $ka$  can be as large as 0.8. We are not aware of any theoretical treatment that simultaneously allows all three parameters to be nonzero. Understanding the regime in which all three parameters are approximately unity is particularly significant because it corresponds to the intriguing roton minimum in the dispersion relation in superfluid liquid He [16, 17]. The behavior in our gas is in some

sense more universal than that in the liquid, because the scattering length is much larger than the range of the interatomic potential [18]. We hope that the results presented below, and follow-up work in progress for lower values of  $k$ , will stimulate interest in the problem.

In Fig. 1, we plot various calculations good to lowest order in combinations of at most two of the three small parameters. Beliaev gives a result for  $ka$  and  $1/(k\xi)$  being nonzero (Eqn. 4.7 in Ref. [19]), and numerical integration of Eqns. 5.13-5.14 in Ref. [19] (see also Ref. [20]) yields a result for  $1/(k\xi)$  and  $\sqrt{8\pi na^3}$  being nonzero; both results are plotted in Fig. 1. We plot also in Fig. 1 the result of a simple model accounting for finite  $ka$  and  $\sqrt{8\pi na^3}$  in the limit of vanishing  $1/(k\xi)$ . Here, Eqn. 1 is modified to become

$$\hbar\omega(k) - \frac{\hbar^2 k^2}{2m} = \frac{8\pi\hbar^2 na(k/2)}{m} - (1 + \alpha) \frac{4\pi\hbar^2 na}{m}. \quad (2)$$

The argument is simply that  $1/(k\xi) \rightarrow 0$  means the excitation  $k$  is very large compared to the momentum content of the correlations induced by nonzero  $\sqrt{8\pi na^3}$ . Thus, for the interaction energy felt by the excitation we ignore many-body corrections and simply use  $8\pi\hbar^2 na(k/2)/m$ , where  $a(k/2) = -\text{Re}(f(k/2))$  and  $f(k/2)$  is the two-body symmetrized scattering amplitude for relative wave vector  $k/2$ . For the energy of an atom in the condensate, we replace  $\mu$  with  $(1 + \alpha)4\pi\hbar^2 na/m$ .

We don't expect Eqn. (2) to be valid in the regime of our experiment, because our value of  $k$  is insufficiently large to ensure the excitations are unaffected by the correlations induced in the condensate by  $\sqrt{8\pi na^3}$  effects. Numerically evaluating the poles of the Green's function, Eqns. 5.13-5.14 in Ref. [19], shows that our Eqn. (2) applies only when  $1/(k\xi) \lesssim 0.05$ , whereas we reach  $1/(k\xi) = 0.5$ . At high momentum (small  $1/(k\xi)$ ), the effect of quantum depletion is to shift the dispersion curve downwards relative to the condensate energy, while at very small momentum, the LHY enhancement to  $\mu$  increases the speed of sound and thus increases low- $k$  values of  $\omega(k)$ . The up-shift due to  $\sqrt{8\pi na^3}$  persists even to the intermediate momenta of our experiment, which is why the dashdotdot curve is above the solid line in Fig. 1.

Our experiments are performed using a  $^{85}\text{Rb}$  BEC near a Feshbach resonance at 155 G [21, 22]. A gas of  $^{85}\text{Rb}$  atoms in the  $|F = 2, m_F = -2\rangle$  state is first sympathetically cooled with  $^{87}\text{Rb}$  in a magnetic trap and then evaporated directly to ultralow temperature in an optical dipole trap [23]. We create a single-species  $^{85}\text{Rb}$  condensate [24], with 40,000 atoms and a condensate fraction greater than 85%, in a weakly confining optical dipole trap at a magnetic field above the Feshbach resonance. Curvature of the magnetic field enhances confinement along the axial direction of the optical trap. Following evaporative cooling, the optical dipole trap is recompressed and the final trap has a measured radial (axial)

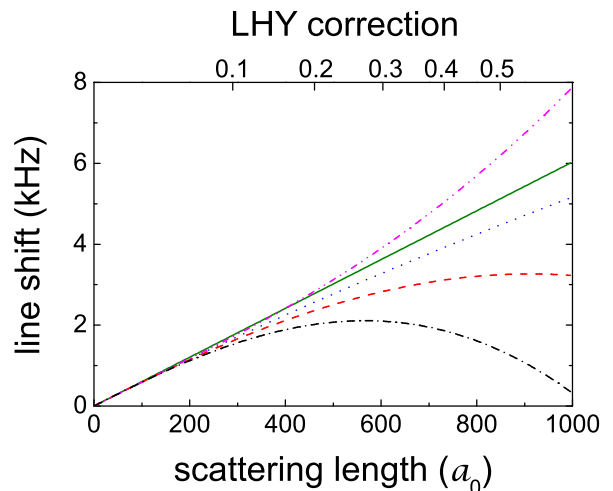


FIG. 1: Theoretical predictions for the peak of the Bragg resonance less the bare kinetic energy for an excitation of wave vector  $k = 2 \frac{2\pi}{780 \text{ nm}}$ , in the case of homogenous density  $7.6 \times 10^{13} \text{ cm}^{-3}$ . The theory lines are described in more detail in the text and correspond to assuming the following quantities are small:  $ka$ ,  $\sqrt{8\pi na^3}$  and  $1/(k\xi)$  (green, solid);  $ka$  and  $\sqrt{8\pi na^3}$  (blue, dots);  $ka$  (magenta, dashdotdot);  $\sqrt{8\pi na^3}$  (red, dashes); and  $1/(k\xi)$  (black, dashdot). For reference the top axis shows the size of the LHY correction,  $\alpha$ , relative to the condensate chemical potential.

trap frequency of  $2\pi \times 134 \text{ Hz}$  ( $2\pi \times 2.9 \text{ Hz}$ ), yielding a condensate mean density of  $2.1 \times 10^{13} \text{ cm}^{-3}$ .

Bragg spectroscopy via stimulated two-photon transitions provides a direct probe of the condensate excitation spectrum. Two counter-propagating, near-resonant laser beams are aligned along the long axis of the condensate. The momentum imparted to a condensate excitation is given by  $\hbar k = 2\hbar k_L$  where  $k_L = \frac{2\pi}{780 \text{ nm}}$  is the wave vector of a beam. The excitation energy is scanned by adjusting the frequency difference of the two laser beams. The average of the two frequencies is red detuned from atomic resonance by 4.2 GHz. The intensity and pulse duration of the Bragg beams are chosen so that the fraction of the condensate excited is less than 10%.

Just before performing the Bragg spectroscopy, we transiently enhance the condensate density by means of large amplitude radial and axial breathing modes, which we excite by modulating the magnetic field and thus the Feshbach-modified scattering length. The rates of the ramps are limited so the  $\dot{a}/a$  never exceeds  $0.06\hbar/(ma^2)$ . The scattering length is derived from measurements of the magnetic field and a previous measurement of the  $^{85}\text{Rb}$  Feshbach resonance [25]. Synchronized with the inner turning point of the radial oscillation, we ramp the scattering length to the value for a given measurement and then pulse on the Bragg beams. During the pulse, the cloud's inward motion is checked and it begins to breathe outward. We model the resulting time-

dependent condensate density using a variational solution to the Gross-Pitaevskii equation [26], which predicts that the density of the cloud does not change by more than 30% during the Bragg pulse. We can meet this goal only by using progressively shorter Bragg pulses for higher values of desired  $a$ . The time- and space-averaged density during the pulse is approximately  $7.6 \times 10^{13} \text{ cm}^{-3}$ , but this depends weakly on the final value of  $a$ .

After the Bragg pulse, we ramp  $a$  to a large, fixed value to ensure that the momentum of the excitations is spread via collisions [27, 28] to the entire condensate sample. We then infer the total momentum, and thus excitation fraction, from the amplitude of the resulting axial slosh, measured via an absorption image taken of the cloud at a time near its axial turning point.

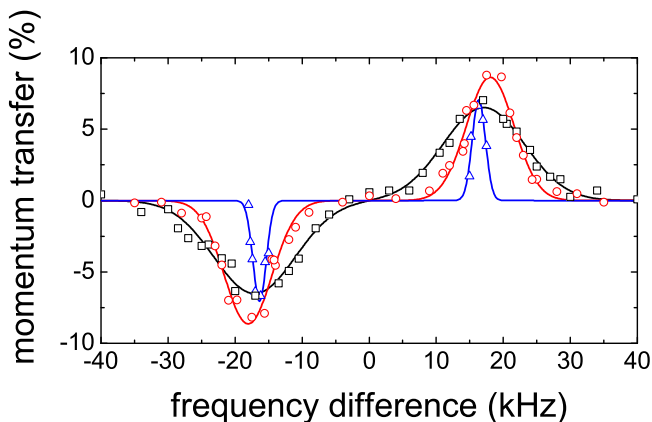


FIG. 2: Typical Bragg spectra at a scattering length of  $100 a_0$  (blue triangles),  $585 a_0$  (red circles), and  $890 a_0$  (black squares). The excitation fraction is determined from the measured momentum transferred to the BEC and plotted as a function of the frequency difference between the two Bragg beams. Lines are fits of the data as described in the text. Mean-field theory predicts a continuous increase in the line shift with increasing  $a$ , however by  $890 a_0$  our data display a *decreasing* shift with stronger interactions.

Figure 2 shows measured Bragg spectra for three values of  $a$ . We fit each Bragg spectrum to an antisymmetric function assuming a Gaussian peak and extract a center frequency and an RMS width. The Bragg line shift is the difference between the fitted center and the ideal gas result  $\frac{1}{2\pi} \frac{\hbar k^2}{2m} = 15.423 \text{ kHz}$ . In Fig. 3a we plot our measured line shifts as a function of the scattering length  $a$ . For  $a \lesssim 300a_0$  (where the predicted LHY correction is already a 10% effect), the measured line shift (● in Fig. 3a) agrees with the simple mean-field result (Eqn. 1). However, as the scattering length is increased further, the resonance line shift deviates significantly from the mean-field prediction. The measured line shift reaches a maximum near  $a = 500a_0$  and then *decreases* as the scattering length is increased further.

At large  $a$  we find that our measured line shift exhibits

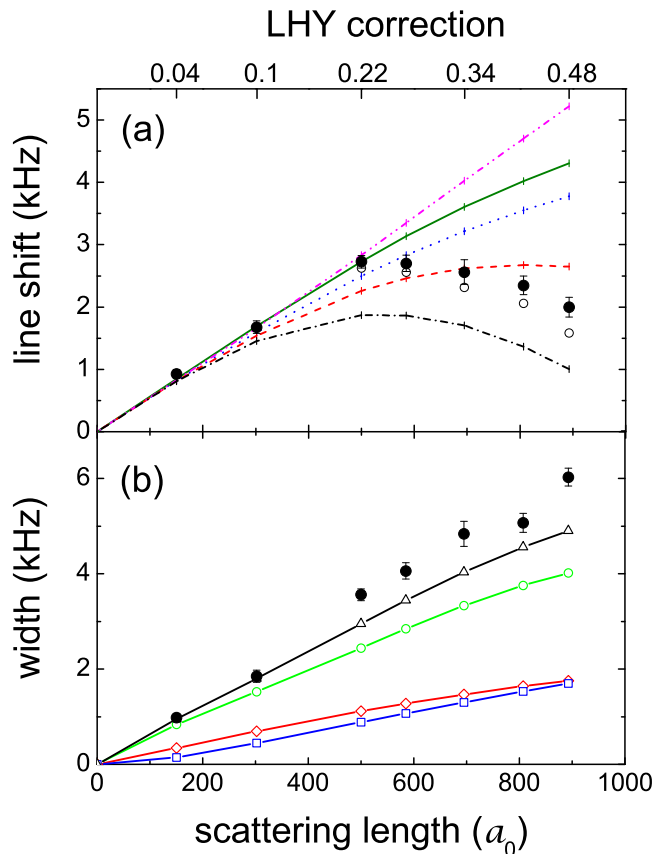


FIG. 3: (a) Bragg line shift and (b) width as a function of scattering length. The hollow circles are our observations. The solid circles are data corrected for a fitting systematic associated with the broad thermal atom background, and the error bars represent fit uncertainties. The theory lines and LHY correction in (a) are as in Fig. 1 except they are calculated for the trapped gas using a local density approximation for each of the corresponding data points; the mean BEC density ranges from  $6.3 \times 10^{13} \text{ cm}^{-3}$  to  $7.6 \times 10^{13} \text{ cm}^{-3}$ . In (b) the solid black circles are the rms width of a gaussian fit to the Bragg spectra. Black triangles are from a fit to a convolution of various contributions to the width calculated under the conditions of our measurements. The remaining symbols characterize constituent contributions to the convolution including the Lorentzian FWHM width due to collisions (blue squares), and the RMS widths of contributions due to the inhomogeneous density (red diamonds) and the pulse duration (green circles). The largest contribution to the width comes from the pulse duration; because the jump to large  $a$  initiates rapid expansion of the BEC, ever shorter pulses are used to obtain the spectra at larger  $a$ .

a systematic dependence on the temperature of the sample [29]. Non-condensed  $^{85}\text{Rb}$  atoms also respond to the Bragg pulse, and this causes an observable effect in the measured line shift when the spectral width of the condensate response becomes comparable to that of the non-condensed atoms (for  $a > 500a_0$ ). We vary the temperature of the gas to characterize this effect and we apply

a small correction to our data to represent the expected line shift at zero temperature ( $\bullet$  in Fig. 3a).

The theory curves of Fig. 1 are adapted for direct comparison with our data (Fig 3a) by calculating, at each tick mark on the curves, a spatial and temporal average over a local density approximation for the corresponding data point, assuming the density of the condensate is given by a time-varying Thomas-Fermi profile. In these predictions, we account for observed number losses (typically  $< 30\%$ ) during our experiments. The observed loss is consistent with the previously observed  $a$ -dependent three-body recombination rate of  $^{85}\text{Rb}$  [22].

Figure 3b shows the measured width of the Bragg peak as a function of  $a$ . Several effects contribute to the total width of the Bragg resonance including the finite duration of the pulse, the inhomogeneous density of the trapped condensate [5], collisions between the excitations and the condensate [27], and Doppler broadening [5]. In our case, Doppler broadening is negligible since the axial size of the condensate is relatively large. To understand the total width we convolve the various calculated lineshapes of the remaining three effects. We fit a Gaussian to the convolution (to match the Gaussian fit to our data) and the RMS width from this fit is shown in Fig. 3b (black  $\triangle$ ). Fig. 3b also shows the expected contributions to the width from each of the three effects. For the lineshape due to collisions we expect a Lorentzian with a full width at half maximum  $\delta\nu = \frac{1}{2\pi} \frac{n\sigma k}{m}$ , where  $\sigma$  is the elastic cross section for collisions between the excitations and low momentum atoms. In calculating  $\sigma$  we include the suppression in the phonon regime predicted by Beliaev [19, 27]. The measured Bragg width exceeds the predicted width in the strongly interacting regime. However, many of the theoretical difficulties in describing the line shift apply also to predicting the width that arises from inhomogeneous density and excitation lifetime.

In comparing our measured line shifts with the various theory models (Fig. 3), one should remember that none of the models takes into account the fact that the inter-atomic potential supports bound states, whose existence means that a Bose-condensed gas can be only a quasi-equilibrium state for any atomic species. This is especially relevant for increasing values of  $a$ . A key future goal of our work is to experimentally explore different time-scales for the establishment of local many-body quasi-equilibrium, and for longer-term evolution. The extreme aspect ratio of our sample hastens the loss of density that occurs during the expansion caused by the ramp to high  $a$ . At present, we are required to use short duration Bragg pulses, which limits our spectral resolution, and we are prevented from tracking the time evolution of line shifts. An ongoing redesign to a more spherical geometry will help. In addition, the Bragg beams are being reconfigured to allow access to the low- $k$ , pure-phonon regime for which  $1/(k\xi) \gg 1$ .

We gratefully acknowledge useful conversations with J.

Bohn, M. Holland, R. Ballagh, S. Stringari and the JILA ultracold atom collaboration. This work is supported by NSF and ONR.

---

\* Email: cornell@jila.colorado.edu

- [1] M. Greiner, O. Mandel, T. Esslinger, T. W. Hänsch, and I. Bloch, *Nature* **415**, 39 (2002).
- [2] E. A. Donley, N. R. Claussen, S. T. Thompson, and C. E. Wieman, *Nature* **417**, 529 (2002).
- [3] C. A. Regal, M. Greiner, and D. S. Jin, *Phys. Rev. Lett.* **92**, 040403 (2004).
- [4] M. W. Zwierlein, C. A. Stan, C. H. Schunck, S. M. F. Raupach, A. J. Kerman, and W. Ketterle, *Phys. Rev. Lett.* **92**, 120403 (2004).
- [5] J. Stenger, S. Inouye, A. P. Chikkatur, D. M. Stamper-Kurn, D. E. Pritchard, and W. Ketterle, *Phys. Rev. Lett.* **82**, 4569 (1999).
- [6] D. M. Stamper-Kurn, A. P. Chikkatur, A. Görlitz, S. Inouye, S. Gupta, D. E. Pritchard, and W. Ketterle, *Phys. Rev. Lett.* **83**, 2876 (1999).
- [7] L. Pitaevskii and S. Stringari, *Phys. Rev. Lett.* **81**, 4541 (1998).
- [8] A. Altmeyer *et al.*, *Phys. Rev. Lett.* **98**, 040401 (2007).
- [9] J. Kinast, A. Turlapov, and J. E. Thomas, *Phys. Rev. A* **70**, 051401(R) (2004).
- [10] F. Dalfovo, S. Giorgini, L. P. Pitaevskii, and S. Stringari, *Rev. Mod. Phys.* **71**, 463 (1999).
- [11] J. Steinhauer, R. Ozeri, N. Katz, and N. Davidson, *Phys. Rev. Lett.* **88**, 120407 (2002).
- [12] R. Ozeri, N. Katz, J. Steinhauer, and N. Davidson, *Rev. Mod. Phys.* **77**, 187 (2005).
- [13] N. Bogolubov, *J. Phys.* **11**, 23 (1947).
- [14] T. D. Lee, and C. N. Yang, *Phys. Rev.* **105**, 1119 (1957).
- [15] T. D. Lee, K. Huang, and C. N. Yang, *Phys. Rev.* **106**, 1135 (1957).
- [16] P. Nozières and D. Pines, *The Theory of Quantum Liquids, Vol. II Superfluid Bose Liquids*, (Addison-Wesley, Redwood City, CA, 1990).
- [17] A. Griffin, *Excitations in a Bose-Condensed Liquid*, (Cambridge University Press, Cambridge, England, 1993).
- [18] E. Braaten, H. W. Hammer, T. Mehen, *Phys. Rev. Lett.* **88**, 040401 (2002).
- [19] S. T. Beliaev, *Sov. Phys. JETP*, **34**, 299 (1958).
- [20] F. Mohling, and A. Sirlin, *Phys. Rev.* **118**, 370 (1960).
- [21] S. L. Cornish, N. R. Claussen, J. L. Roberts, E. A. Cornell, and C. E. Wieman, *Phys. Rev. Lett.* **85**, 1795 (2000).
- [22] J. L. Roberts, N. R. Claussen, S. L. Cornish, and C. E. Wieman, *Phys. Rev. Lett.* **85**, 728 (2000).
- [23] S. B. Papp and C. E. Wieman, *Phys. Rev. Lett.* **97**, 180404 (2006).
- [24] The number of trapped  $^{87}\text{Rb}$  atoms remaining is  $< 10\%$  of the  $^{85}\text{Rb}$  number.
- [25] N. R. Claussen, S. J. J. M. F. Kokkelmans, S. T. Thompson, E. A. Donley, E. Hodby, and C. E. Wieman, *Phys. Rev. A* **67**, 060701(R) (2003).
- [26] V. M. Pérez-García, H. Michinel, J. I. Cirac, M. Lewenstein, and P. Zoller, *Phys. Rev. A* **56**, 1424 (1997).
- [27] N. Katz, J. Steinhauer, R. Ozeri, and N. Davidson, *Phys.*

- Rev. Lett. **89**, 220401 (2002).
- [28] A. P. Chikkatur, A. Görlitz, D. M. Stamper-Kurn, S. Inouye, S. Gupta, and W. Ketterle, Phys. Rev. Lett. **85**, 483 (2000).
- [29] A. Brunello, F. Dalfovo, L. Pitaevskii, S. Stringari, and F. Zambelli, Phys. Rev. A **64**, 063614 (2001).